Communication in Physical Sciences, 2026, 13(11) :1738-1758f

Effect of Chloride Concentration on the Electrochemical Corrosion of Iron Embedded in Cement-Based Concrete: An Integrated Study Using Electrochemical Techniques

Ayodeji Ajidahun
Received: : 18 August 2026/ Accepted: 25 September 2026/Published: 01 October 2026
DOI: 10.4314/cps.v13i11.3

Abstract: *This study investigated the electrochemical corrosion behaviour of iron embedded in concrete under control, low-chloride, and high-chloride conditions using electrochemical impedance spectroscopy (EIS), potentiodynamic polarization, linear polarization resistance (LPR), and open-circuit potential (OCP) measurements. The results indicated a progressive reduction in impedance with increasing chloride exposure. The approximate low-frequency impedance difference decreased from 67.99 kΩ·cm² in the control to 31.55 kΩ·cm² under low-chloride conditions and 12.57 kΩ·cm² under high-chloride conditions, representing reductions of 53.6% and 81.5%, respectively. The illustrative potentiodynamic parameters showed an increase in corrosion current density from 0.18 µA/cm² in the control to 0.82 µA/cm² and 2.15 µA/cm² under low- and high-chloride conditions, respectively. Similarly, the estimated polarization resistance decreased from 144.4 kΩ·cm² to 31.7 kΩ·cm² and 12.1 kΩ·cm², corresponding to reductions of 78.1% and 91.6%, respectively. OCP measurements revealed potential shifts of −8.59 mV, −38.59 mV, and −28.59 mV over 60 minutes for the control, low-chloride, and high-chloride conditions, respectively, with the high-chloride condition maintaining the most negative potential. Collectively, these trends suggest that increasing chloride exposure reduces the electrochemical resistance of iron in concrete and may promote destabilization of its protective passive film. However, some numerical parameters are illustrative and have not been independently verified against the original experimental measurements. Equivalent-circuit fitting, validated Tafel analysis, and appropriate Stern–Geary calculations are therefore required before definitive corrosion-rate estimates can be established.*

Keywords*: Iron corrosion; chloride concentration; concrete reinforcement; electrochemical impedance spectroscopy; polarization resistance.*

Ayodeji Ajidahun
Federal University of Technology, Akure
Ondo State, Nigeria
Email: dejiajidahun@gmail.com
https://orcid.org/0009-0001-2520-9631

1.0 Introduction

Reinforced concrete is widely used in civil engineering infrastructure because of its strength, durability, and versatility. Its long-term performance, however, depends partly on the ability of concrete to protect embedded steel against corrosion (Eddy, 2010: Eddy & Ita, 2011). Under normal conditions, the highly alkaline pore solution of concrete promotes the formation of a protective passive film on the steel surface. The presence of chloride ions can destabilize this film, initiate localized corrosion, and ultimately contribute to reinforcement deterioration, concrete cracking, delamination, and loss of structural durability (Bertolini *et al*., 2013; Glass & Buenfeld, 2000).

Chloride-induced corrosion is particularly important in marine environments, coastal structures, and infrastructure exposed to chloride-contaminated materials (Isu, 2019). The severity of corrosion depends on chloride

concentration, concrete composition, moisture, oxygen availability, and the condition of the steel–concrete interface. Angst *et al.* (2009) reported substantial variability in the critical chloride content required to initiate corrosion, indicating that corrosion behaviour cannot be predicted from chloride concentration alone. Understanding the electrochemical response of iron under different chloride conditions is therefore essential for assessing its susceptibility to corrosion in concrete.

Electrochemical techniques provide complementary approaches for investigating corrosion. Electrochemical impedance spectroscopy (EIS) characterizes the frequency-dependent impedance response of the system, while potentiodynamic polarization provides information on corrosion potential and current density when appropriate analysis is possible. Linear polarization resistance (LPR) assesses resistance to small potential perturbations, and open-circuit potential (OCP) monitoring tracks changes in electrode potential over time. When interpreted together, these methods provide a broader assessment of corrosion behaviour than any single technique (Bertolini *et al*., 2013).

Despite extensive research on chloride-induced corrosion, differences in experimental conditions and the limitations of individual electrochemical methods complicate comparisons of corrosion behaviour across chloride exposure levels. In particular, impedance, polarization resistance, current density, and electrode potential represent different aspects of the electrochemical system and must be interpreted collectively. This study therefore investigates the electrochemical corrosion behaviour of iron embedded in concrete under control, low-chloride, and high-chloride conditions using EIS, potentiodynamic polarization, LPR, and OCP measurements. The study aims to compare the electrochemical responses across these conditions and establish how chloride exposure is associated with changes in impedance, polarization resistance, corrosion-related current response, and potential stability. The findings may contribute to understanding chloride-associated corrosion susceptibility and inform further research on the durability of reinforced concrete structures.

2.0 Materials and Methods

2.1. Materials and Experimental Conditions

The study investigated the electrochemical corrosion behaviour of iron embedded in concrete under three exposure conditions: control, low-chloride, and high-chloride conditions. The control condition served as the reference for evaluating changes associated with chloride exposure, while the low- and high-chloride conditions were used to examine the influence of increasing chloride concentration on the electrochemical response of the iron–concrete system.

The experimental materials comprised iron specimens, concrete constituents, and chloride-containing materials used to establish the exposure conditions. The iron specimens were evaluated in the concrete environment to simulate the interaction between embedded iron and the surrounding cementitious matrix. The specific iron composition, specimen dimensions, concrete mix proportions, chloride source, and chloride concentrations should be reported from the original experimental records.

2.2. Preparation of Iron–Concrete Specimens

Iron specimens were embedded in concrete prepared for the three exposure conditions. The control specimens were maintained without deliberate chloride addition, while chloride was introduced into the low- and high-chloride conditions according to the experimental design. To ensure meaningful comparisons, specimen preparation, exposed surface area, curing conditions, and environmental exposure should be kept consistent across the three conditions, except for the intended difference in chloride concentration.



Before electrochemical measurements, the specimens were conditioned under the prescribed experimental environment. The exposed iron surface and electrical connections were prepared to provide reliable electrical contact and minimize interference from unintended exposed areas. Details of specimen surface preparation, curing duration, chloride incorporation procedure, and conditioning time should be included once confirmed from the laboratory records.

2.3. Electrochemical Measurements

Electrochemical measurements were performed using electrochemical impedance spectroscopy (EIS), potentiodynamic polarization, linear polarization resistance (LPR), and open-circuit potential (OCP) techniques. These methods were used to evaluate impedance characteristics, corrosion-related current response, polarization resistance, and potential variation under the three chloride conditions.

2.3.1. Electrochemical Impedance Spectroscopy

EIS was used to characterize the frequency-dependent response of the iron–concrete system. The impedance spectra were evaluated using Nyquist and Bode plots. Nyquist plots were used to examine the relationship between the real and imaginary components of impedance, while Bode plots were used to assess impedance magnitude and phase angle as functions of frequency.

The high-frequency real-axis intercept was used as an estimate of the uncompensated resistance. The low-frequency impedance response was compared across the three conditions to evaluate changes in the overall electrochemical impedance. Where appropriate, equivalent-circuit fitting should be applied to estimate interfacial parameters such as charge-transfer resistance. Approximate differences obtained directly from selected Nyquist coordinates were not treated as independently fitted charge-transfer resistance.

2.3.2. Potentiodynamic Polarization

Potentiodynamic polarization was used to investigate the relationship between electrode potential and current density under the different chloride conditions. The resulting polarization curves were compared to assess differences in corrosion potential and electrochemical current response.

Where suitable linear regions were identifiable on the anodic and cathodic branches of a potential-versus-logarithmic-current-density plot, Tafel extrapolation could be used to estimate corrosion current density. The validity of the estimated parameters depends on the quality of the polarization data and the suitability of the selected fitting regions. Consequently, corrosion potential and corrosion current density should be reported as experimentally determined parameters only after verification using the original polarization data (Eddy *et al*., 2019).

2.3.3. Linear Polarization Resistance

LPR measurements were used to assess the resistance of the iron–concrete system to small potential perturbations around the corrosion potential. The polarization resistance was obtained from the inverse slope of the current-density–potential relationship near the corrosion potential based on equation 1

$$R_p = \left(\frac{di}{dE}\right) \quad (1)$$

where R_p is polarization resistance, i is current density, E is electrode potential, and . When current density is normalized by the exposed electrode area, the resulting polarization resistance is expressed in area-normalized units.

The resistance values were compared across the control, low-chloride, and high-chloride conditions. Where validated anodic and cathodic Tafel slopes were available, corrosion current density could be estimated using the Stern–Geary relationship. Without a validated Stern–Geary constant, the LPR results were interpreted in terms of polarization resistance rather than as definitive corrosion rates.

2.3.4. Open-Circuit Potential

OCP measurements were used to monitor changes in the electrode potential over time without an externally imposed current. The potential was recorded over a 60-minute monitoring period for the control, low-chloride, and high-chloride conditions.

The net potential change was calculated as the difference between the potential at 60 minutes and the initial potential as shown in equation 2 (Ameh *et al*., 2016)_

$$\Delta E_{OCP} = E_{60} - E_0 \qquad (2)$$

where E_{60} is the potential measured after 60 minutes and E_0 is the initial potential. The resulting changes were compared to evaluate potential stability under the different chloride conditions. The reference electrode used for the measurements should be identified, and all reported potentials should be expressed against that same reference.

2.4. Data Processing and Comparative Analysis

The electrochemical results were compared using the parameters obtained from each measurement technique. For EIS, the analysis considered the high-frequency resistance, low-frequency impedance response, impedance magnitude, and phase angle. For potentiodynamic polarization, the relevant parameters were corrosion potential and, where reliably determined, corrosion current density. For LPR, the principal parameter was polarization resistance, while OCP analysis focused on the initial potential, final potential, net potential change, and minimum recorded potential.

Percentage changes relative to the control were calculated using equation 3

$$\%\, Change = \frac{X_{control} - X_{condition}}{X_{control}} \times \frac{100}{1} \qquad (3)$$

where X represents the parameter being compared. For parameters expected to decrease, such as impedance or polarization resistance, percentage reduction was calculated using the control value minus the condition value in the numerator.

The results were interpreted by comparing trends across the three exposure conditions and examining whether the electrochemical techniques provided consistent evidence of changes in corrosion susceptibility. Particular attention was given to distinguishing measured values from parameters calculated from the supplied data and to avoiding direct corrosion-rate conclusions where the underlying assumptions or analytical procedures had not been validated.

2.5. Quality Assurance and Limitations

Reliable comparison of the three chloride conditions requires consistent specimen preparation, exposed surface area, environmental conditions, and measurement procedures. The reference electrode, instrument settings, frequency range, polarization scan rate, potential perturbation, and chloride concentrations should be documented from the original experimental records to support reproducibility.

Some values used in the preliminary analysis were illustrative rather than independently verified experimental measurements. Accordingly, they should be confirmed against the original data before being presented as experimental findings. Equivalent-circuit fitting should be used where charge-transfer resistance is reported, Tafel parameters should be derived from appropriate regression of the polarization curves, and corrosion-rate calculations based on LPR should use a justified Stern–Geary constant.

3.0 Results and Discussion

3.1. Electrochemical Impedance Spectroscopy: Nyquist Plots

Electrochemical impedance spectroscopy (EIS) was used to evaluate the corrosion behaviour of iron embedded in concrete under low- and high-chloride conditions, using the control condition as a reference. The Nyquist plots provide information about the resistance of the concrete–iron system to electrochemical reactions and the behaviour of the iron–

concrete pore-solution interface. In these plots, the real component of impedance (\(Z'\)) is plotted against the negative imaginary component (\(-Z''\)). The high-frequency intercept is associated primarily with the ohmic resistance of the concrete pore solution and other resistive contributions, whereas the diameter of a well-defined capacitive arc can provide an estimate of the charge-transfer resistance at the iron interface.

The supplied Nyquist data indicate a progressive decrease in the high-frequency real-axis intercept from approximately 45 $\Omega.cm^2$ for the control to 35 $\Omega.cm^2$ under low chloride and 25 $\Omega.cm^2$ under high chloride. Relative to the control, these values represent decreases of approximately 22.2% and 44.4%, respectively. This reduction suggests a change in the ohmic resistance of the concrete–electrolyte system as chloride exposure increases. However, the intercept may also be affected by concrete moisture content, pore-solution conductivity, temperature, and the electrode configuration; it should therefore not be attributed solely to corrosion of the embedded iron.

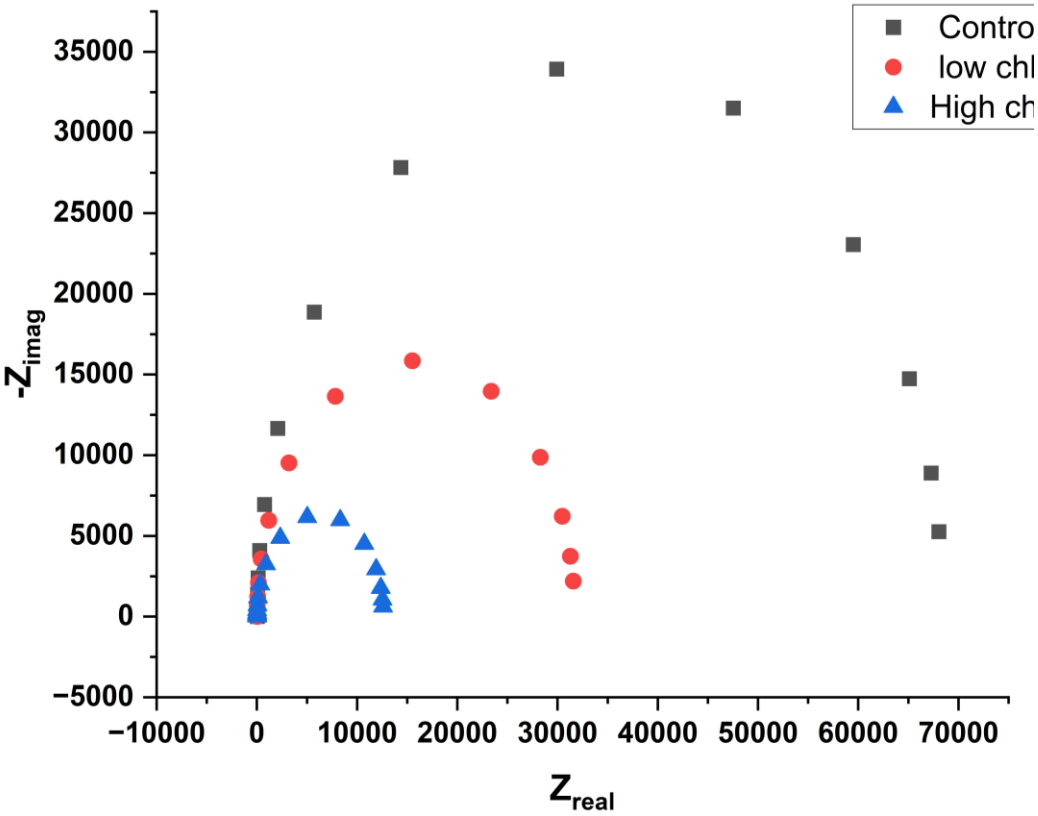


Fig. 1: Nyquist plots of iron embedded in concrete under control, low-chloride, and high-chloride conditions

A more pronounced difference is observed in the low-frequency impedance response. The approximate low-frequency real impedance is substantially higher for the control than for either chloride-exposed condition. After subtracting the high-frequency intercept, the resulting impedance differences are approximately 67.99, 31.55, and 12.57 $k\Omega.cm^2$ \ for the control, low-chloride, and high-chloride conditions, respectively. These differences correspond to reductions of approximately 53.6% under low chloride and 81.5% under high chloride relative to the control. The impedance difference was calculated using equation 4.

$$R_{diff} = Z'_{LF} - R_s \quad (4)$$

where Z'_{LF} is the low-frequency real impedance and R_s is the estimated high-frequency resistance. The percentage reduction was calculated using equation (5):

$$\%Reduction = \frac{R_{control} - R_{condition}}{R_{control}} \times \frac{100}{1} \quad (5)$$

The calculated values are recorded in Table 1 to compare the relative changes in impedance as the chloride condition changes.

Table 1: Comparison of impedance characteristics under different chloride conditions. Placement in manuscript: Immediately after the discussion of the calculated impedance differences.

Parameter	Control	Low chloride	High chloride
High-frequency intercept, \(R_s\) (Ω·cm²)	45	35	25
Approximate low-frequency impedance difference (kΩ·cm²)	67.99	31.55	12.57

The results in Table 1 show that the control has the largest impedance difference, while the high-chloride condition has the smallest. The low-chloride condition exhibits an intermediate response. This pattern suggests that increasing chloride concentration is associated with a progressive reduction in the impedance of the iron–concrete system, particularly at low frequencies, where interfacial electrochemical processes may contribute substantially to the measured response.

The observed trend is relevant to the corrosion of reinforcing iron in concrete. Under normal conditions, the high alkalinity of concrete promotes the formation and maintenance of a protective passive film on the iron surface. Chloride ions penetrating the concrete can disrupt this film locally, particularly when the chloride concentration at the steel surface exceeds the level that the passive layer can tolerate. Depassivation can initiate localised corrosion, resulting in anodic dissolution of iron and associated cathodic reactions. As corrosion develops, the electrochemical response of the interface may change, leading to a reduction in the measured low-frequency impedance.

The substantially lower impedance difference under high chloride is therefore consistent with a system exhibiting greater electrochemical activity than the control. The low-chloride condition also shows a considerable reduction, suggesting that even the lower chloride exposure may influence the response of the iron–concrete interface. Nevertheless, the magnitude of this effect depends on the actual chloride concentration, concrete composition, water content, oxygen availability, exposure duration, and condition of the iron surface. The supplied values do not establish the chloride threshold for depassivation or prove that active corrosion has occurred.

It is also important to distinguish the approximate impedance difference in Table 1 from the charge-transfer resistance, \(R_{ct}\). The former was calculated by subtracting the high-frequency intercept from the low-frequency real impedance. Although this can

provide a useful comparative indicator, it is not automatically equivalent to \(R_{ct}\). A defensible estimate of charge-transfer resistance requires analysis of the measured Nyquist response using an appropriate equivalent circuit, with the relevant arcs and frequency ranges adequately resolved.

Overall, the Nyquist results suggest that the electrochemical response of iron embedded in concrete becomes less resistive as chloride concentration increases, with the strongest change under high-chloride conditions. If verified by experimental measurements and suitable equivalent-circuit fitting, this trend would support the interpretation that higher chloride exposure increases the susceptibility of reinforcing iron to electrochemical corrosion.

3.1.2. Bode Plots: Impedance Magnitude and Phase Angle

Bode plots were used to examine the frequency-dependent impedance magnitude and phase-angle response of iron embedded in concrete under control, low-chloride, and high-chloride conditions. Unlike Nyquist plots, which display the relationship between the real and imaginary components of impedance, Bode plots illustrate how the magnitude and phase angle vary across the applied frequency range. These responses provide complementary information on the resistive and capacitive characteristics of the electrochemical system and help assess changes associated with chloride exposure.

3.1.2.1. Bode Impedance Magnitude

The Bode impedance magnitude represents the absolute value of complex impedance at a given frequency. It is calculated from the real and imaginary components using equation (6):

$$|Z| = \sqrt{|Z'|^2 + |Z''|^2} \qquad (6)$$

where $|Z|$ is the impedance magnitude, $|Z'|$ is the real component, and Z'' is the imaginary component of impedance. Where the impedance is normalized by the exposed electrode area, it is expressed in Ω.cm^2.

Fig. 2 presents the Bode impedance magnitude as a function of frequency for the control, low-chloride, and high-chloride conditions. The comparison focuses particularly on the low-frequency response, which may be sensitive to interfacial electrochemical processes, including charge transfer and transport phenomena.

The illustrative low-frequency impedance magnitudes are approximately 68.24, 31.66, and 12.61 Ω.cm^2 for the control, low-chloride, and high-chloride conditions, respectively. The control therefore exhibits the highest impedance magnitude, while the high-chloride condition exhibits the lowest. This trend is consistent with the reduction in the approximate low-frequency impedance difference observed in the Nyquist analysis.

The percentage reduction (%R) in impedance magnitude relative to the control was calculated using equation 5:

$$\%R = \frac{|Z|_{control} - |Z|_{condition}}{|Z|_{control}} \times \frac{100}{1} \qquad (7)$$

For the low-chloride condition, the recorded reduction was 53.60%, while the high-chloride condition gave 81.50% reduction. These calculations indicate an approximate 53.6% reduction in low-frequency impedance magnitude under low-chloride exposure and an 81.5% reduction under high-chloride exposure relative to the control.

The progressive decrease in impedance magnitude suggests that the electrochemical system offers less opposition to alternating current as chloride concentration increases. In iron embedded in concrete, this behaviour may be associated with changes in the passive film, the steel–concrete interface, and the conductivity of the surrounding concrete pore solution. Chloride ions can destabilize the passive film and promote localized corrosion, potentially increasing interfacial electrochemical activity.

However, impedance magnitude reflects the combined response of the electrochemical system rather than a single corrosion parameter. It can be influenced by concrete resistivity, moisture content, electrode geometry, and interfacial processes. Consequently, the reduction in \(|Z|\) is consistent with chloride-associated changes in electrochemical behaviour but does not, by itself, quantify the corrosion rate or establish the value of the charge-transfer resistance.

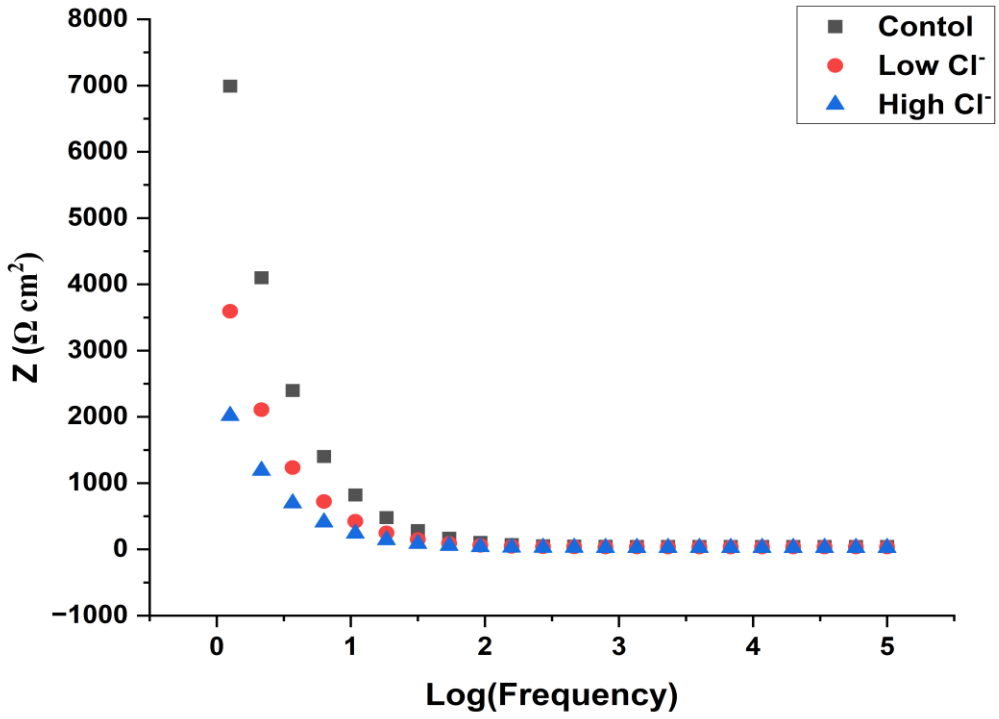


Fig. 2: Bode impedance magnitude as a function of frequency for iron embedded in concrete under control, low-chloride, and high-chloride conditions

3.1.2.2. Bode Phase-Angle Response

The phase-angle response provides additional information about the relative resistive and capacitive behaviour of the electrochemical interface. Complex impedance can be expressed according to equation 8 while the phase angle was calculated using equation 9

$$Z = Z' + jZ'' \quad (8)$$

$$\emptyset = tan^{-1}\left(\frac{Z''}{Z'}\right) \quad (9)$$

The sign of the phase angle depends on the convention used for the imaginary component. Under the common convention in which capacitive impedance has a negative imaginary component, capacitive responses have negative phase angles.

Fig. 3 compares the phase-angle response of iron embedded in concrete under the three chloride conditions. The plot should show frequency in hertz on a logarithmic horizontal axis and phase angle in degrees on the vertical axis.

From Fig. 3, the minimum phase angles are approximately 87, 86, and 85 ° for the control, low-chloride, and high-chloride conditions, respectively. These values show relatively small differences among the conditions, with the minimum phase angle becoming slightly

less negative as chloride concentration increases.

Phase angles approaching 90 ° generally indicate strongly capacitive behaviour over the relevant frequency range. The values presented therefore suggest that a substantial capacitive contribution remains in all three conditions. Nevertheless, the small shift towards less negative values may reflect changes in interfacial capacitance, surface heterogeneity, passive-film characteristics, or the distribution of electrochemical relaxation processes.

Under chloride exposure, localized breakdown of the passive film may produce a more heterogeneous steel surface, potentially altering the capacitive response. However, the minimum phase angle alone cannot establish the extent of passive-film deterioration. Interpretation should also consider the frequency at which the minimum occurs, the width of the phase-angle response, and the corresponding impedance magnitude.

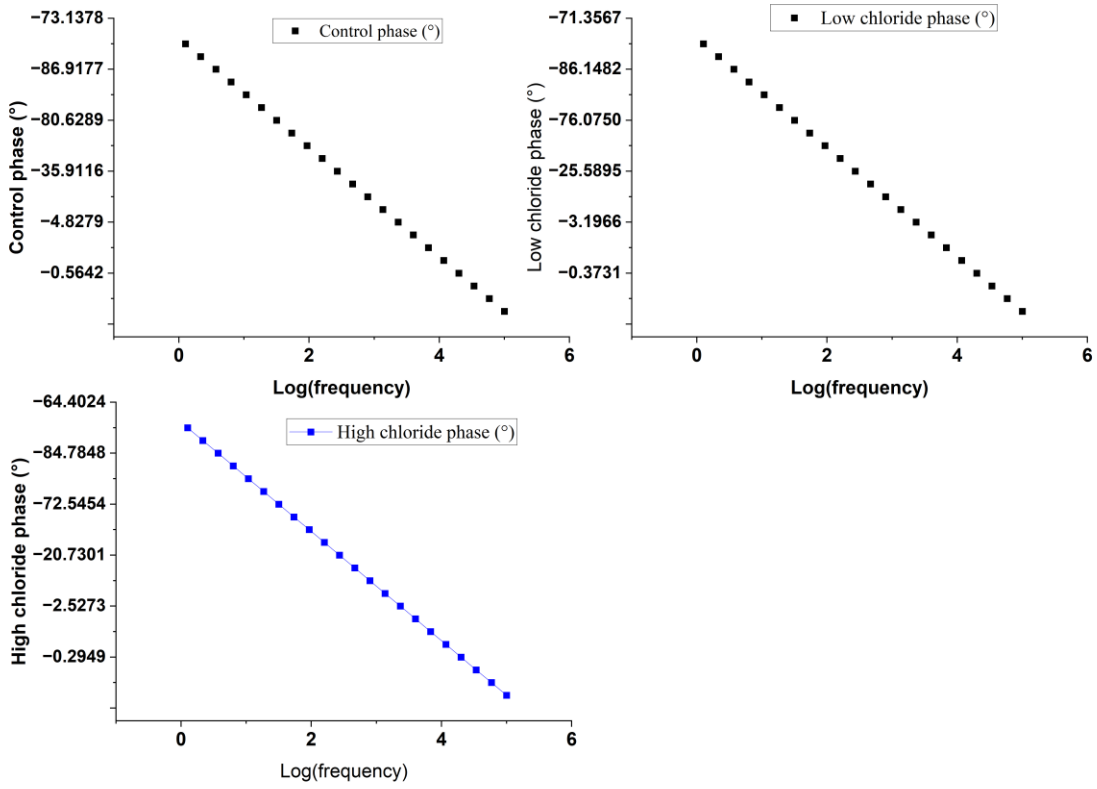


Fig. 3: Bode phase angle as a function of logarithmic frequency for the control, low-chloride, and high-chloride conditions

For an idealized interface represented by a parallel combination of charge-transfer resistance and double-layer capacitance, the characteristic frequency can be expressed according to equation 10

$$f_{max} = \frac{1}{2\pi R_{ct} C_{dl}} \quad (10)$$

where f_{max} is the characteristic frequency in hertz, R_{ct} is the charge-transfer resistance in ohms, and C_{dl} is the double-layer capacitance in farads. This equation assumes a simple single-time-constant response. More complex steel–concrete interfaces may exhibit multiple relaxation processes and non-ideal capacitive behaviour, requiring a more comprehensive

equivalent-circuit model. Because the characteristic frequency depends on both resistance and capacitance, a shift in frequency cannot be attributed exclusively to a change in either parameter without further analysis.

3.1.2.3. Comparative Analysis of Bode Parameters

Table 2 summarizes the illustrative low-frequency impedance magnitudes and minimum phase angles for the three chloride conditions. The table facilitates direct comparison of the magnitude of the impedance changes and the relatively small variation in phase angle.

Table 2 demonstrates a substantial reduction in low-frequency impedance magnitude with increasing chloride exposure. The low-chloride condition shows an intermediate response, whereas the high-chloride condition exhibits the largest reduction. The approximately 81.5% reduction under high-chloride exposure indicates a markedly different impedance response from that of the control. In contrast, the minimum phase angles differ by only 2 ° across the three conditions. This suggests that the change in impedance magnitude is more pronounced than the change in the minimum phase angle in the illustrative dataset. The two parameters therefore provide complementary rather than interchangeable information: impedance magnitude reflects the overall opposition to alternating current, whereas phase angle describes the relative resistive and capacitive characteristics of the system.

The similarity of the phase-angle minima does not necessarily contradict the large differences in impedance magnitude. An electrochemical system may retain a predominantly capacitive response while its impedance magnitude changes substantially. Accordingly, both parameters should be evaluated together, and the complete frequency-dependent spectra should be considered before assigning specific interfacial mechanisms.

Table 2 : Comparison of Bode impedance magnitude and minimum phase angle under different chloride conditions

Parameter	Control	Low Cl^-	High Cl^-
Low-frequency impedance magnitude ($\Omega.cm^2$)	68.24	31.66	12.61
Minimum phase angle (°)	−87	−86	−85
Reduction in impedance magnitude relative to control (%)	—	53.6	81.5

3.1.2.4. Implications for Chloride-Induced Corrosion of Iron in Concrete

The Nyquist and Bode analyses indicate a consistent trend in the dataset: impedance decreases as chloride exposure increases. The control exhibits the highest impedance response, the low-chloride condition shows an intermediate response, and the high-chloride condition exhibits the lowest impedance magnitude. This pattern is consistent with increased electrochemical activity and possible destabilization of the passive film protecting iron embedded in concrete.

The findings are relevant to reinforced concrete because chloride-induced corrosion can lead to metal loss and the accumulation of corrosion products around reinforcement. The resulting internal stresses may contribute to cracking, delamination, and deterioration of the bond between steel and concrete. However, the impedance results alone do not demonstrate that these physical effects have occurred; additional corrosion-rate measurements and concrete-condition assessments would be needed.

3.2. Potentiodynamic Polarization Analysis

Potentiodynamic polarization measurements were used to investigate the corrosion

behaviour of iron embedded in concrete under control, low-chloride, and high-chloride conditions. Unlike electrochemical impedance spectroscopy (EIS), which characterizes the frequency-dependent response of the electrochemical system, potentiodynamic polarization examines the relationship between applied electrode potential and current density. The resulting polarization curves provide information about the corrosion potential, \(E_{\mathrm{corr}}\), corrosion current density, \(i_{\mathrm{corr}}\), and the anodic and cathodic reactions occurring at the iron–concrete interface.

These parameters are particularly important in reinforced concrete because corrosion of embedded iron involves the oxidation of iron and the simultaneous reduction of an oxidizing species, commonly dissolved oxygen. Chloride ions can destabilize the passive film that normally protects steel in the alkaline pore solution of concrete, potentially promoting localized corrosion. Comparing polarization behaviour under different chloride conditions therefore helps assess the extent to which chloride exposure may influence the electrochemical activity of iron.

3.2.1. Potentiodynamic Polarization Curves

Fig. 4 presents the potentiodynamic polarization curves for the control, low-chloride, and high-chloride conditions. The curves should be plotted as electrode potential against the logarithm of current density, with anodic and cathodic branches identified where possible. The corrosion potential is associated with the mixed potential at which the total anodic and cathodic currents are equal in magnitude.

The electrochemical parameters for the three conditions are presented in Table 3. They indicate a progressive shift in corrosion potential towards more negative values and an increase in corrosion current density with increasing chloride concentration.

Table 3. Illustrative potentiodynamic polarization parameters under different chloride conditions.

Parameter	Control	Low Cl^-	High Cl^-
Corrosion potential (E (mV vs Ag/AgCl)	−250	−350	−425
Corrosion current density ($\boldsymbol{i_{corr}}$ (μA/cm²)	0.18	0.82	2.15
Increase in \$\boldsymbol{i_{corr}}$ relative to control (%)	—	355.6	1,094.4
Approximate current density ratio relative to control	1.0	4.6	11.9

The corrosion current density provides an indication of the rate of electrochemical corrosion under suitable measurement conditions. Its relative increase was calculated using equation 11 (Eddy *et al*., 2015)

$$\%\ increase = \frac{i_{corr,control} - i_{corr,condition}}{i_{corr,control}} \times \frac{100}{1} \quad (11)$$

Based on equation 9, the results obtained for the low-chloride condition was 355.6% while the high-chloride condition was 1,094.4\% . These results indicate that the corrosion current density under low-chloride exposure is approximately 4.6 times that of the control, while the value under high-chloride exposure is approximately 11.9 times that of the control. If confirmed experimentally, such increases would indicate substantially greater corrosion-related electrochemical activity under chloride exposure, particularly at the higher concentration.

The illustrative corrosion potential decreases from −250 mV in the control to −350 mV under low-chloride exposure and −425 mV under high-chlorid exposure, all referenced to

Ag/AgCl. This shift towards more negative potentials suggests a change in the mixed electrochemical state of the iron–concrete system as chloride concentration increases.

In concrete, the corrosion potential reflects the combined effects of anodic iron dissolution and cathodic reactions, together with the local chemical environment, oxygen availability, moisture content, and condition of the passive film. Chloride-induced disruption of passivity may alter the balance between these reactions and shift the measured corrosion potential.

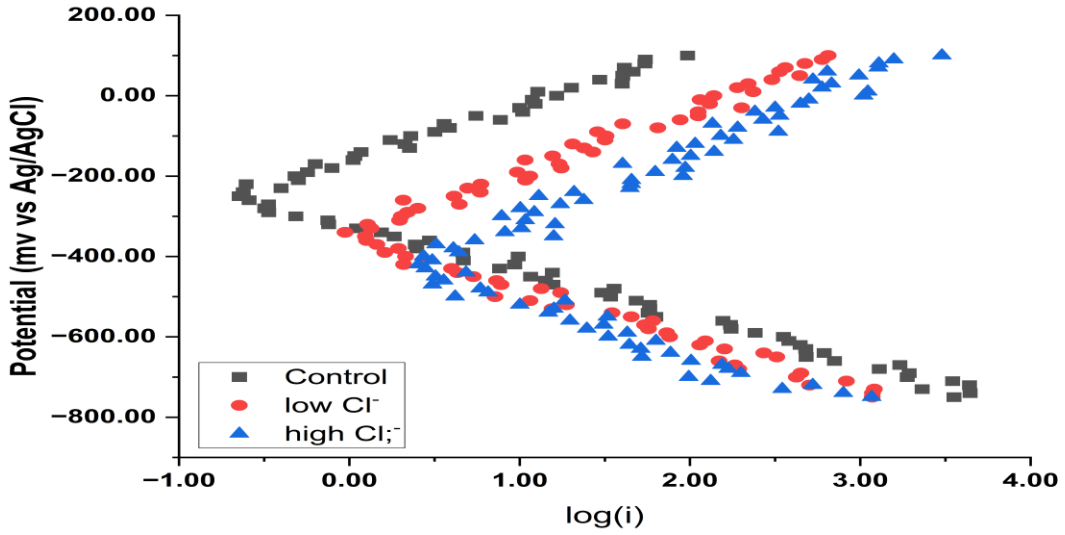


Fig. 4: Potentiodynamic polarization curves of iron embedded in concrete under control, low-chloride, and high-chloride conditions

However, a more negative corrosion potential does not, on its own, demonstrate a higher corrosion rate. Corrosion potential indicates the electrochemical tendency of the system, whereas corrosion current density is more directly associated with the corrosion rate when determined reliably. Interpretation of the potential shift must also account for the reference electrode used and the environmental conditions during measurement.

In this case, the simultaneous negative shift in E_{corr} and increase in the illustrative i_{corr} would be consistent with a transition towards more active corrosion behaviour under increasing chloride exposure. The corrosion current density trend, if confirmed by valid polarization analysis, provides the stronger basis for comparing the relative corrosion activity of the three conditions.

Where the anodic and cathodic branches contain sufficiently linear regions on a potential-versus-log-current-density plot, the Tafel method can be used to estimate the corrosion current density. The anodic and cathodic Tafel relationships may be expressed as equation 10 and 11 respectively (Eddy *et al*., 2026a, b).

$$\eta_a = \beta_a \left(\frac{i_a}{i_{corr}}\right) \quad (12)$$

$$\eta_c = \beta_c \left(\frac{i_c}{i_{corr}}\right) \quad (13)$$

where η_a and η_c are the anodic and cathodic overpotentials, respectively; β_a and β_c are the anodic and cathodic Tafel slopes; i_a and i_c are the corresponding partial current densities; and i_{corr} is the corrosion current density. Also, overpotential is defined according to equation 14

$$\eta = E - E_{corr} \quad (14)$$

where E is the applied electrode potential and E_{corr} is the corrosion potential. The corrosion current density is estimated by extrapolating the linear portions of the anodic and cathodic Tafel branches to the corrosion potential. The slopes and intersection should be obtained from regression of the actual experimental data rather than assigned from the illustrative parameters.

The olarization parameters show two important trends: the corrosion potential shifts towards more negative values, and the corrosion current density increases as chloride concentration rises. If these trends are confirmed by the original measurements, they would support the interpretation that chloride exposure increases corrosion-related electrochemical activity at the iron–concrete interface.

Under the control condition, the alkaline concrete pore solution is expected to favour the formation and maintenance of a passive film on iron. This film limits the rate of iron dissolution and helps preserve the reinforcement. Under low-chloride exposure, chloride ions may initiate localized breakdown at susceptible points in the film, allowing anodic dissolution to occur. Under high-chloride exposure, a greater availability of chloride ions may increase the likelihood of passive-film breakdown and sustain more active corrosion sites.

The anodic dissolution process can be represented by equation 16 9Eddy *et al*., 2008)

$$Fe \rightarrow Fe^{2+} + 2e^{-} \qquad (15)$$

In the presence of oxygen and water, a common cathodic reaction in aerated concrete as illustrated by equation 1 (Odoemelam *et al*., 2008)

$$O_2 + 2H_2O + 4e^{-} \rightarrow 4OH^{-} \qquad (16)$$

The electrons released during iron oxidation are consumed by cathodic reactions, allowing corrosion to proceed. Chloride ions facilitate localized attack by destabilizing passivity and participating in the chemistry of corrosion sites; they are not themselves the oxidizing agent in these reactions.

Based on the corrosion current densities in Table 3, Faraday's law can be used to estimate the 8corresponding average iron penetration rate according to equation 18 (Recha, 2026).

$$v = \frac{i_{corr} M_{Fe}}{nF\rho_{Fe}} \qquad (17)$$

where v is the penetration rate in cm/s when consistent centimetre-based units are used, i_{corr} is in A/cm², M_{Fe} is the molar mass of iron (55.845 g/mol), n is the number of electrons exchanged per iron atom, F is Faraday's constant (approximately 96,485 C/mol), and ρ_{Fe} is the density of iron (approximately 7.87 g/cm³). The experimental data suggest greater corrosion activity under high-chloride exposure than under low-chloride exposure or the control.

3.3. Linear Polarization Resistance (LPR) Analysis

Linear polarization resistance (LPR) measurements were used to assess the resistance of iron embedded in concrete to small changes in applied electrode potential under control, low-chloride, and high-chloride conditions. The technique involves applying a small potential perturbation around the open-circuit or corrosion potential and measuring the resulting current response. The polarization resistance provides an indication of the electrochemical resistance to corrosion reactions and can be used to estimate corrosion current density when an appropriate Stern–Geary constant is available.

LPR is particularly relevant to reinforced concrete because the corrosion of embedded iron can be influenced by chloride-induced breakdown of the passive film, concrete resistivity, moisture availability, and oxygen transport. Comparing polarization resistance across the three conditions therefore provides additional information on the possible influence of chloride concentration on the corrosion behaviour of iron.

3.3.1. Linear Polarization Response

Fig. 5 presents the current-density response to changes in applied potential for the control,

low-chloride, and high-chloride conditions. The slope of the current-density–potential relationship near the corrosion potential is used to determine polarization resistance.

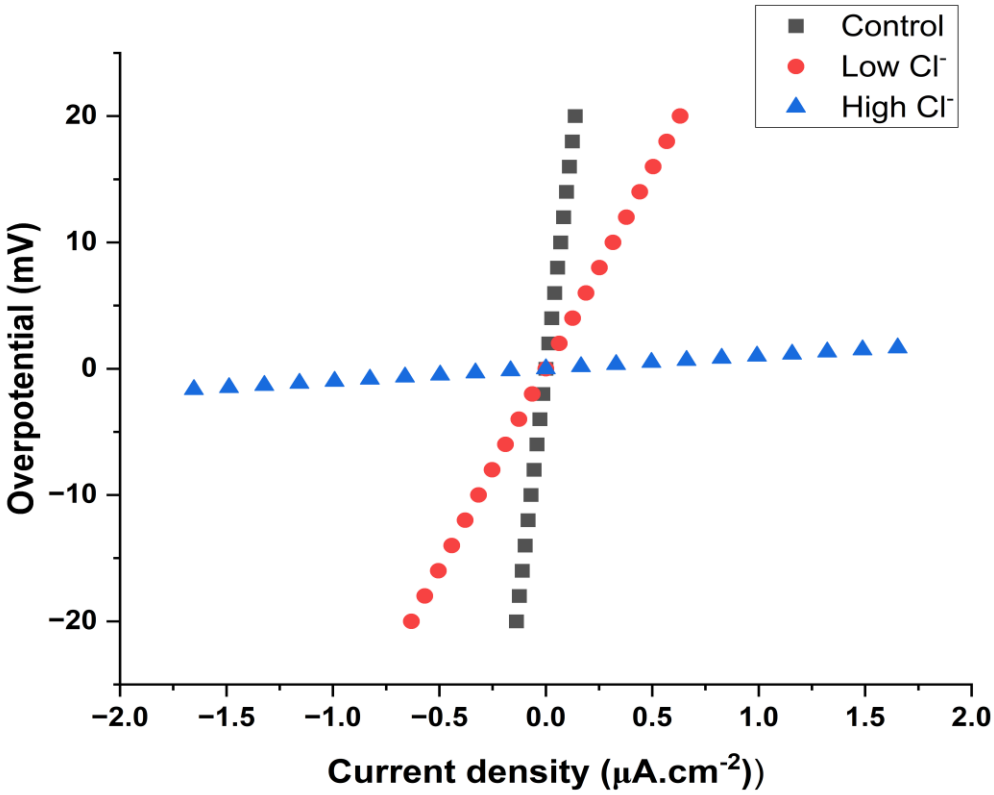


Fig. 5: Current density–overpotential curves of iron embedded in concrete under control, low-chloride, and high-chloride conditions.

The slope of the current-density response is calculated using equation 18

$$S = \left(\frac{di}{dE}\right)_{E\sim E_{corr}} \quad (18)$$

where S is the slope of current density, i, with respect to electrode potential, E, near the corrosion potential. Polarization resistance is the inverse of this slope, which can also be written as

$$R_p = \left(\left(\frac{di}{dE}\right)_{E\sim E_{corr}}\right)^{-1} \quad (19)$$

where R_p is expressed in Ω.cm^2 when current density is area-normalized and potential is expressed in volts. The supplied observed current-density–potential data give slopes of approximately 0.006925, 0.031545, and 0.082645 Ω.cm^{-2} for the control, low-chloride, and high-chloride conditions, respectively. The corresponding polarization resistances are approximately 144.4, 31.7, and 12.1 Ω.cm^2. These values indicate a progressive decrease in polarization resistance as chloride concentration increases. The control exhibits the highest resistance, whereas the high-chloride condition exhibits the lowest. If confirmed experimentally, this trend would suggest that the iron–concrete interface offers less resistance to electrochemical reactions under increased chloride exposure.

3.3.2. Comparison of Polarization Resistance

The percentage reduction in polarization resistance relative to the control was calculated using equation 19

Table 4 shows that the illustrative polarization resistance decreases by approximately 78.1% under low-chloride exposure and 91.6% under high-chloride exposure relative to the control.

The high-chloride condition therefore exhibits the greatest reduction in resistance to polarization.

$$\%Reducetion = \frac{R_{p,control} - R_{p.condition}}{R_{p,control}} \times \frac{100}{1} \quad (21)$$

The calculated results are summarized in Table 4.

Table 4. Comparison of polarization resistance under different chloride conditions

Parameter	Control	Low chloride	High chloride
Current-density–potential slope	0.006925	0.031545	0.082645
Polarization resistance (R_p)	144.4	31.7	12.1
Reduction in $R_p$relative to control (%)	—	78.1	91.6

For iron embedded in concrete, this trend is consistent with chloride-associated deterioration of electrochemical protection. Under alkaline conditions, a passive film normally limits the dissolution of iron. Chloride ions can destabilize this film locally, allowing anodic dissolution to (proceed at susceptible sites. A lower polarization resistance is consistent with a system in which a small potential change produces a larger change in current density, indicating a more responsive electrochemical interface.

3.3.3. Relationship Between Polarization Resistance and Corrosion Current Density

The Stern–Geary equation relates polarization resistance to corrosion current density according to equation 20

$$i_{corr} = \frac{B}{R_p} \quad (21)$$

where $i_{corr}$is the corrosion current density, R_p is the polarization resistance, and B is the Stern–Geary constant. The constant can be estimated from the anodic and cathodic Tafel slopes according to equation 23 (Akpanudo, 2026)

$$B = \frac{\beta_a \beta_c}{2.304(\beta_a + \beta_c)} \quad (22)$$

where $\beta\ and_a\beta_c$ are the anodic and cathodic Tafel slopes, respectively, expressed in compatible potential-per-decade units.

Equations (20) and (21) show that, for a constant and valid B a reduction in polarization resistance corresponds to an increase in corrosion current density. However, a numerical corrosion current density cannot be established from the supplied LPR values alone because independently validated Tafel slopes, and hence a suitable Stern–Geary constant, have not been provided.

This limitation is particularly important for iron in concrete because chloride exposure may change the condition of the passive film and the kinetics of the anodic and cathodic reactions. Consequently, the Stern–Geary constant may not be identical across all three conditions. Applying one assumed constant to every condition without justification could introduce substantial uncertainty into the estimated corrosion rates.

3.3.4. Implications for Corrosion of Iron in Concrete

The illustrative LPR results indicate that polarization resistance decreases substantially as chloride concentration increases. The control exhibits the highest \(R_p\), followed by the low-chloride condition, while the high-chloride condition exhibits the lowest \(R_p\). This pattern is consistent with a progressive reduction in the electrochemical resistance of the iron–concrete system under chloride exposure.

In reinforced concrete, the loss of passivity can permit iron dissolution, resulting in corrosion-product formation and eventual deterioration of the reinforcement. If corrosion progresses, the accumulation of corrosion products may exert pressure on the surrounding concrete, contributing to cracking, delamination, and

loss of steel–concrete bond. These are potential consequences of sustained corrosion, not effects demonstrated directly by the polarization-resistance data.

The LPR trend is also broadly consistent with the illustrative EIS results, which show lower impedance under increased chloride exposure. Agreement between these independent electrochemical techniques would strengthen the interpretation that chloride exposure increases corrosion activity. However, the comparison remains provisional until the underlying measurements are verified and the relevant parameters are calculated using appropriate analytical methods.

Overall, the supplied LPR data suggest that high-chloride exposure is associated with the greatest reduction in polarization resistance, indicating potentially greater corrosion susceptibility of iron embedded in concrete. Experimental confirmation, correction for relevant resistance contributions, and application of the Stern–Geary relationship using validated parameters are necessary before quantitative corrosion-rate conclusions can be drawn.

3.4. Open-Circuit Potential (OCP) Analysis

Open-circuit potential (OCP) measurements were used to investigate the electrochemical stability of iron embedded in concrete under control, low-chloride, and high-chloride conditions over a period of 60 minutes. OCP is the potential measured when no externally imposed current is applied to the electrode. Monitoring its variation with time provides information about the stabilization of the iron–concrete interface and changes in its electrochemical state during exposure.

In reinforced concrete, the OCP response is influenced by the condition of the passive film, chloride concentration, moisture content, oxygen availability, and the chemical environment surrounding the embedded iron. Chloride-induced destabilization of passivity can shift the measured potential towards more negative values. However, OCP is an indicator of electrochemical tendency rather than a direct measurement of corrosion rate; its interpretation should therefore be supported by EIS, polarization, and LPR results.

3.4.1. Variation of Open-Circuit Potential with Time

Fig. 6 shows the variation in measured potential with exposure time for the three conditions. The control maintains the most positive potential throughout the monitoring period, the low-chloride condition exhibits an intermediate potential, and the high-chloride condition maintains the most negative potential.

The control potential decreases from approximately −125 mV at the beginning of monitoring to around −134 mV at 60 minutes, indicating a relatively small potential drift. The low-chloride condition exhibits a larger negative shift, from approximately −285 mV to −324 mV, while the high-chloride condition shifts from approximately −425 mV to −454 mV. The curves gradually approach relatively stable values towards the end of the monitoring period, although complete electrochemical stabilization cannot be established from the potential trend alone.

The differences between the three curves indicate that the electrochemical state of the iron–concrete interface varies substantially with chloride exposure. The increasingly negative potentials under low- and high-chloride conditions are consistent with changes in the surface condition of the iron and possible destabilization of its protective passive film. Nevertheless, potential shifts may also be influenced by oxygen availability, moisture, and other environmental factors.

3.4.2. Calculation of OCP Parameters

The net change in open-circuit potential over the monitoring period was calculated using equation 23

$$\Delta E_{OCP} = E_{60} - E_0 \qquad (23)$$

where E_0 is the initial potential and E_{60} is the potential after 60 minutes. A negative value

indicates a shift towards a more negative potential.The calculations gave -8.49, -38.59 and -28.59 mV for the control condition, low chloride condition and high chloride condition respectively.

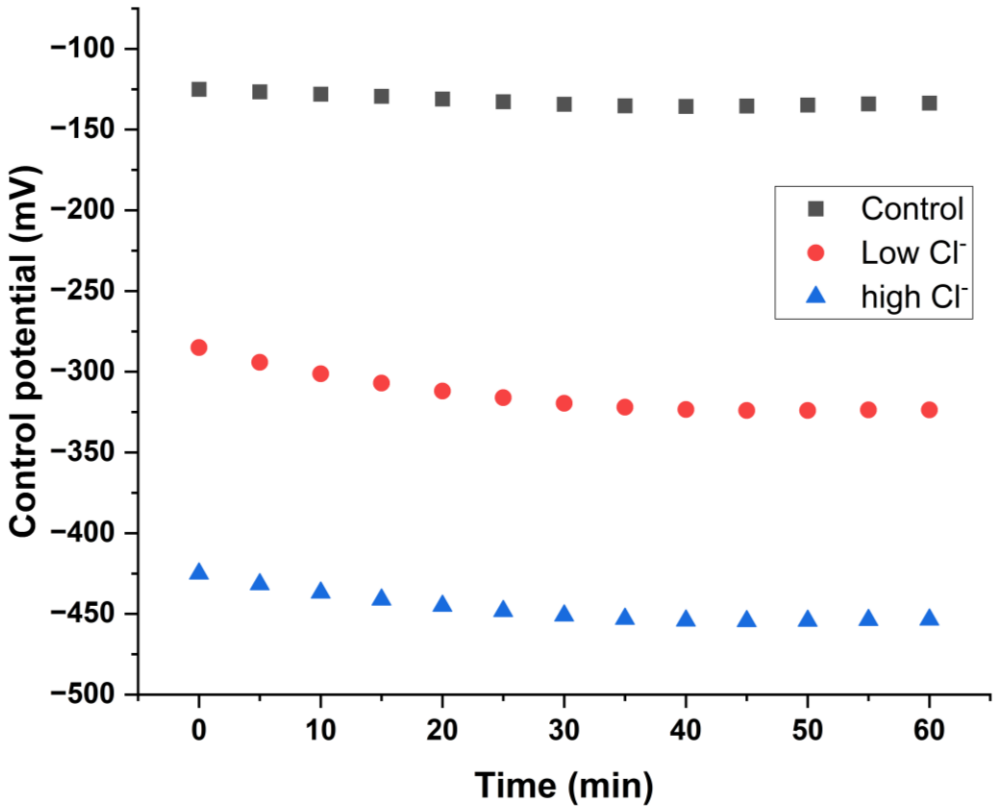


Fig. 6: Variation in open-circuit potential of iron embedded in concrete under control, low-chloride, and high-chloride conditions over 60 minutes.

The magnitude of the potential change was compared with that of the control using equation 25

$$Relative\ drift\ (\%) = \frac{|\Delta E_{condition}|}{|\Delta E_{control}|} \times \frac{100}{1} \quad (25)$$

For the low-chloride condition, the result obtained is 449.1%, but for high chloride condition the drift was 332.8%. These percentages compare the magnitude of potential drift; they are not percentages of corrosion rate or corrosion probability. The above calculated parameters are summarized in Table 5.

3.4.3. Discussion of the OCP Results in Relation to Iron Corrosion in Concrete

Table 5 reveals three important features of the OCP response. First, the control exhibits the smallest net potential drift, at −8.59 mV. This relatively limited change suggests that the electrochemical state of the iron–concrete interface is comparatively stable during the monitoring period. Under suitable alkaline conditions, iron can maintain a passive oxide film that restricts further metal dissolution. The relatively small potential shift is consistent with this possibility, although OCP alone cannot confirm the integrity of the passive film. Second, the low-chloride condition exhibits the largest net potential drift, at −38.59 mV, which is approximately 4.49 times the magnitude of the control drift. This result indicates a greater change in the measured electrochemical state

during the 60-minute period. Chloride ions may destabilize susceptible regions of the passive film, allowing local anodic dissolution to develop. The larger drift is consistent with a changing iron–concrete interface, but it does not establish that the low-chloride condition has the highest corrosion rate.

Table 5. Summary of open-circuit potential parameters under different chloride conditions

Parameter	Control	Low chloride	High chloride
Initial potential, E_0 (mV)	−125.00	−285.00	−425.00
Potential at 60 min, E_{60}	−133.59	−323.59	−453.59
Net potential change,ΔE_{OCP} (mV)	−8.59	−38.59	−28.59
Magnitude of potential drift relative to control (%)	100.0	449.1	332.8
Minimum recorded potential (mV)	−135.68	−323.99	−454.47
Time of minimum potential (min)	40	45	45

Third, the high-chloride condition has the most negative absolute potential throughout the monitoring period and a net drift of −28.59 mV. Although its potential drift is smaller than that of the low-chloride condition, its absolute potential is substantially more negative. This distinction is important: the magnitude of potential drift describes how much the potential changes during monitoring, whereas the absolute potential describes the measured electrochemical state relative to the reference electrode. Consequently, the low-chloride condition shows the greatest change from its initial potential, while the high-chloride condition maintains the most negative potential. These findings are not contradictory because the two measurements describe different characteristics of the electrochemical response.

For iron embedded in concrete, the more negative potential under high-chloride exposure is consistent with a potentially more active corrosion state and possible chloride-induced loss of passivity. However, the measured potential is also affected by oxygen availability, moisture, concrete chemistry, and the reference electrode.

3.4.4. Relationship Between OCP and the Other Electrochemical Measurements

The OCP results should be interpreted alongside the EIS, potentiodynamic polarization, and LPR findings. The illustrative EIS data show a substantial reduction in impedance with increasing chloride concentration, while the supplied polarization parameters suggest increasing corrosion current density. The LPR data also indicate decreasing polarization resistance as chloride concentration increases.

If these trends are confirmed experimentally, their combined interpretation would support the conclusion that chloride exposure reduces the electrochemical protection of iron embedded in concrete and increases its susceptibility to corrosion. The OCP results add useful information by showing that the high-chloride condition maintains the most negative potential, while the low-chloride condition experiences the largest potential drift during the monitoring period.

The combined evidence is more informative than any individual technique. EIS characterizes the frequency-dependent impedance response; polarization measurements can help estimate corrosion kinetics when analysed appropriately; LPR measures the resistance to small potential perturbations; and OCP tracks the evolution of

the electrode's electrochemical potential without externally imposed current.

Overall, the OCP measurements demonstrate distinct electrochemical responses under the three chloride conditions. The control exhibits the smallest potential drift, the low-chloride condition exhibits the largest drift, and the high-chloride condition maintains the most negative potential. These observations are consistent with chloride-associated changes in the condition of iron embedded in concrete, but quantitative corrosion-rate conclusions must be based on validated polarization or LPR analysis supported by the EIS results.

4.0 Conclusion

This study investigated the electrochemical corrosion behaviour of iron embedded in concrete under control, low-chloride, and high-chloride conditions using electrochemical impedance spectroscopy (EIS), potentiodynamic polarization, linear polarization resistance (LPR), and open-circuit potential (OCP) measurements. The combined results indicate that chloride exposure is associated with substantial changes in the electrochemical response of the iron–concrete system, with the high-chloride condition generally exhibiting the strongest indications of reduced electrochemical resistance and increased corrosion susceptibility.

The EIS results showed a progressive decrease in impedance with increasing chloride exposure. The approximate low-frequency impedance difference decreased from 67.99 kΩ·cm² in the control to 31.55 kΩ·cm² under low-chloride exposure and 12.57 kΩ·cm² under high-chloride exposure. These values correspond to reductions of approximately 53.6% and 81.5%, respectively, relative to the control. The Bode impedance magnitude exhibited a similar trend, supporting the interpretation that chloride exposure reduces the impedance response of the system. This behaviour is consistent with possible destabilization of the protective passive film and increased electrochemical activity at the iron–concrete interface. However, the impedance differences are approximate and should not be interpreted as fitted charge-transfer resistance without equivalent-circuit analysis.

The potentiodynamic polarization parameters also indicated a progressive change with chloride concentration. The illustrative corrosion current density increased from 0.18 μA/cm² in the control to 0.82 μA/cm² under low-chloride exposure and 2.15 μA/cm² under high-chloride exposure. These values represent increases of approximately 355.6% and 1,094.4%, respectively, relative to the control. The corrosion potential also shifted towards more negative values, from −250 mV in the control to −350 mV and −425 mV under low- and high-chloride conditions, respectively, relative to Ag/AgCl. If validated through appropriate analysis of the original polarization curves, these trends would support increased corrosion-related electrochemical activity under chloride exposure.

The LPR results further suggested a reduction in resistance to polarization as chloride concentration increased. The illustrative polarization resistance decreased from 144.4 kΩ·cm² in the control to 31.7 kΩ·cm² under low-chloride exposure and 12.1 kΩ·cm² under high-chloride exposure. These changes correspond to reductions of approximately 78.1% and 91.6%, respectively. The trend is consistent with the EIS observations and suggests that the high-chloride condition may offer the least resistance to electrochemical reactions. Nevertheless, quantitative corrosion-rate estimates require validated polarization resistance measurements and an appropriate Stern–Geary constant.

The OCP measurements revealed distinct potential responses among the three conditions. The control exhibited the smallest potential drift, at −8.59 mV over 60 minutes, while the low-chloride and high-chloride conditions showed shifts of −38.59 mV and −28.59 mV, respectively. The high-chloride condition

maintained the most negative potential throughout the monitoring period, whereas the low-chloride condition exhibited the largest net potential change. These findings demonstrate that the absolute potential and the magnitude of potential drift describe different aspects of the electrochemical response. Although the more negative potential under high-chloride exposure is consistent with a potentially more active corrosion state, OCP alone cannot establish the corrosion rate.

The results suggest that increasing chloride concentration adversely affects the electrochemical protection of iron embedded in concrete. The observed reductions in impedance and polarization resistance, together with the illustrative increase in corrosion current density, are consistent with chloride-induced destabilization of the passive film and an increased susceptibility to corrosion. Such deterioration, if sustained, could contribute to reinforcement loss and the eventual degradation of reinforced concrete through corrosion-product accumulation, cracking, and loss of steel–concrete bond.

5.0 References

Akpanudo, N. W. (2026). Electrochemical performance and corrosion protection of zinc–carbon quantum dot (Zn–CQD) nanocomposite coatings on mild steel. *Communication in Physical Sciences*, 13, 7, pp. 1116–1138.

Ameh, P. O., & Eddy, N. O. (2016). Theoretical and experimental studies on the corrosion inhibition potentials of 3-nitrobenzoic acid for mild steel in 0.1 M H_2SO_4. *Cogent Chemistry*, *2, 1, pp.* 1–18. https://doi.org/10.1080/23312009.2016.1253904

Angst, U., Elsener, B., Larsen, C. K., & Vennesland, Ø. (2009). Critical chloride content in reinforced concrete—A review. *Cement and Concrete Research*, 39, 12, pp. 1122–1138. https://doi.org/10.1016/j.cemconres.2009.08.006

Bertolini, L., Elsener, B., Pedeferri, P., Redaelli, E., & Polder, R. B. (2013). *Corrosion of steel in concrete: Prevention, diagnosis, repair* (2nd ed.). Wiley-VCH. https://doi.org/10.1002/9783527651696

Eddy, N. O. (2010). Adsorption and inhibitive properties of ethanol extract of *Garcinia kola* and *Cola nitida* for the corrosion of mild steel in H_2SO_4. *Pigment & Resin Technology*, *39*(6), 348–354.

Eddy, N. O., Ameh, P. O., & Essien, N. B. (2018). Experimental and computational chemistry studies on the inhibition of aluminium and mild steel in 0.1 M HCl by 3-nitrobenzoic acid. *Journal of Taibah University for Science*, *12*(5), 545–556. https://doi.org/10.1080/16583655.2018.1500514

Eddy, N. O., Ekwumemgbo, P., & Odoemelam, S. A. (2008). Inhibition of the corrosion of mild steel in H_2SO_4 by 5-amino-1-cyclopropyl-7-[(3R,5S)-3,5-dimethylpiperazin-1-yl]-6,8-difluoro-4-oxo-quinoline-3-carboxylic acid (ACPDQC). *International Journal of Physical Sciences*, *3*(11), 275–280.

Eddy, N. O., Eze, I. S., Adukwu, I. D., Garg, R., Garg, R., Taziwa, R., & Watandost, H. (2026a). Synthesis and characterization of limestone derived biphasic calcium silicate nanocomposites for coating and fuel cell applications. *Discover Materials*. https://doi.org/10.1007/s43939-026-00819-9

Eddy, N. O., & Ita, B. I. (2011). Experimental and theoretical studies on the inhibition potentials of some derivatives of cyclopenta-1,3-diene for the corrosion of mild steel in HCl solutions. *International Journal of Quantum Chemistry*, *111*(14), 3456–3474.

Eddy, N. O., Momoh-Yahaya, H., & Oguzie, E. E. (2015). Theoretical and experimental studies on the corrosion inhibition potentials of some purines for aluminum in 0.1 M HCl. *Journal of Advanced Research*, 6, 2, pp. 203–216. https://doi.org/10.1016/j.jare.2014 .01.004

Eddy, N. O., Nweze, S., Eze, I. S., Garg, R., Taziwa, R., & Watandost, H. (2026b). Synthesis, characterisation and electrochemical behaviour of calcium carbonate nanoparticles derived from automobile oxy-acetylene gas welding waste. *Discover Nano*, 21, 1, Article 360. https://doi.org/10.1186/s11671-026-04796-z

Glass, G. K., & Buenfeld, N. R. (2000). Chloride-induced corrosion of steel in concrete. *Progress in Structural Engineering and Materials*, 2, 4, pp. 448–458. https://doi.org/10.1002/pse.54

Issa, M. O. (2019). Electrochemical investigation of chloride-induced corrosion of steel reinforcement in reinforced concrete under accelerated laboratory conditions. *Communication in Physical Sciences*, 4, 2, pp. 188–207. https://doi.org/10.5281/zenodo.21549661

Odoemelam, S. A., & Eddy, N. O. (2008). Effect of pyridoxal hydrochloride-2,4-dinitrophenyl hydrazone on the corrosion of mild steel in HCl. *Journal of Surface Science and Technology*, 24, 3, pp.

Recha, F. (2026). Estimation of corrosion current density considering the uncertainty of the model parameters. *Civil and Environmental Engineering*, *22*(1), 282–293. https://doi.org/10.2478/cee-2026-0028

Declarations

Funding

The author declared no external sources kf funding

Conflict of Interest

The author declared no conflict of interest

Data Availability

Data shall be made available upon request

Ethical Considerations

Not applicable

Author Contributions

All components of the work were written by the author.